N91-22998

EVOLUTION OF THE OLYMPUS MONS CALDERA, MARS

Peter J. Mouginis-Mark[1]; Mark S. Robinson[1]; and Maria T. Zuber[2]. 1: Planetary Geosciences Division, SOEST, Univ. Hawaii, Honolulu, HI, 96822; 2: Code 621 Goddard Space Flight Center, Greenbelt, MD 20771.

Extensive high-resolution (15 - 20 m/pixel) coverage of Olympus Mons volcano permits the investigation of the sequence of events associated with the evolution of the nested summit caldera, thereby extending our previous study (1). The sequence of intra-caldera events is well illustrated by image data collected on orbits 473S and 474S of Viking Orbiter 1 (Fig. 1a). These data cover both the oldest and youngest portions of the caldera floor. Our observations permit the following chronology for the caldera floor to be inferred, which in turn can be interpreted in terms of the internal structure of the volcano (i.e., magma chamber depth, existence of dikes; ref. 2, 3):

Stage 1: The first preserved summit event was the catastrophic collapse and subsequent partial infilling of crater #1 (Fig. 1b). Our own shadow length measurements of the preserved wall (Viking frame 890A68, 156 m/pixel) indicate that at least 1,100 ± 60 m of collapse took place. Wall material from this collapse is now buried beneath younger materials. **Stage 2**: Subsidence across the entire caldera floor promoted the formation of the radial and concentric ridges similar to lunar mare ridges (Fig. 2). Continued subsidence (~1,300 ± 120 m of displacement) of the central portion of crater #1 created an extensional environment close to caldera wall and a compressional environment closer to caldera center. Concentric graben and ridges formed on the floor (Fig. 2). The transition from graben to ridges (local extension to compression) occurs at a radial distance of ~17 km from the center of the 65 km diameter caldera, and has been used to infer the magma chamber depth (2, 3). **Stage 3**: New collapse events occurred to the west, forming crater #3. A similar episode of circumferential graben formation took place within this portion of the caldera. **Stage 4**: Additional new collapse events just south of the caldera center post-date graben formation within craters #1 and 3. **Stage 5**: On the basis of morphologic evidence for resurfacing, during (or just after) its formation, the combined floor of craters 4 and 5 was probably occupied by a large lava lake. Linear ridges formed on surface that are interpreted to be compressional features produced by local convergence (rafting) on the lake surface. These ridges (Fig. 3) cross boundaries of craters 4 & 5, indicating that both craters were flooded (and, by inference, were convectively overturning) at the same time. **Stage 6**: Partial drainage of the lava lake surface produced a bench around perimeter of crater 4. **Stage 7**: Continued subsidence of entire summit area produced a compressional environment that promoted the formation of large (>3 km wide) wrinkle ridges in craters 1, 2 and 5 (Fig. 3). The numerous linear ridges formed in Stage 6 are now preserved on top of these larger wrinkle ridges. **Stage 8**: Final collapse event of ~350 m displacement produces crater #6. There is no evidence of surface features that could be associated with dynamic overturn of the lava lake on this crater floor. Nor is there any evidence of subsequent tectonic deformation.

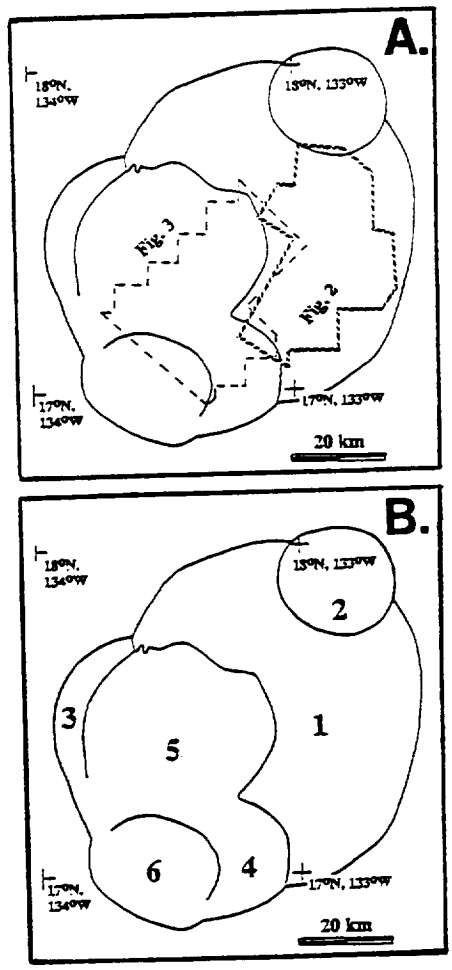

Fig. 1a (Top): Data coverage from Orbits 437S (Fig. 3) and 474S (Fig. 2). Fig. 1b (Bottom): Sequence of caldera collapse episodes. "1" oldest, "6" youngest (ref. 1).

This sequence of events demonstrates that Olympus Mons underwent a protracted period of summit activity. While all segments of the caldera floor possess craters that are interpreted to be impact in origin, no pronounced difference in crater size/frequency curves has been observed for different segments of the caldera floor, implying that all of the observed events probably occurred in a relatively short period of martian history.

References:
1) Mouginis-Mark, P. J. (1981), Proc. Lunar Planet. Sci., **12B**, p. 1431 - 1447. 2) Zuber, M. T. and Mouginis-Mark, P.J. (1989). *Proc. MEVTV Conf. on Tectonic Features on Mars*, LPI, Houston. 3) Zuber, M.T. and Mouginis-Mark P.J. (1990) This vol.

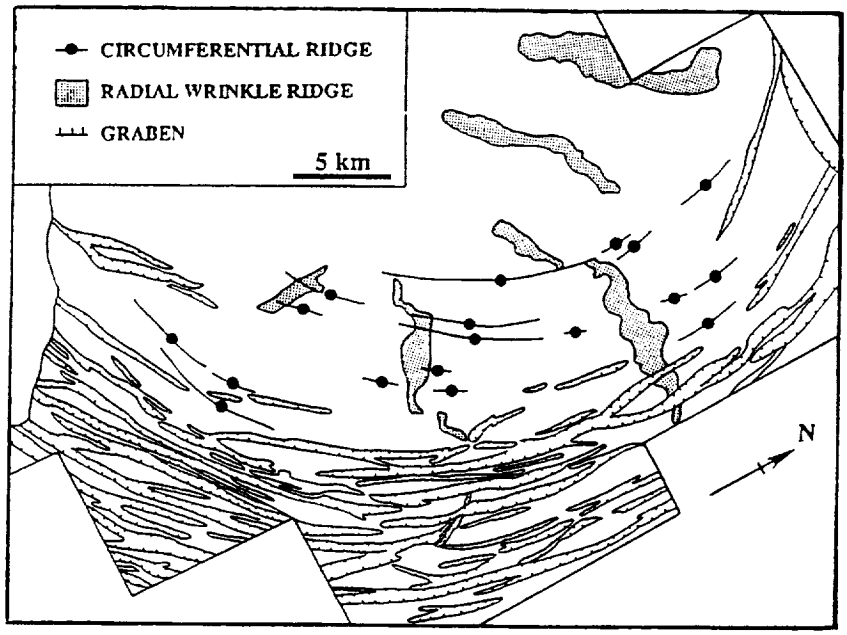

Fig. 2 (Top): Distribution of circumferential graben and ridges within the oldest portion (crater #1) of the Olympus Mons caldera. Note that these graben are truncated by the wall to crater #4. See Fig. 1a for location. Mapped from Viking Orbiter frames 473S27 - 29, 474S25 - 30.

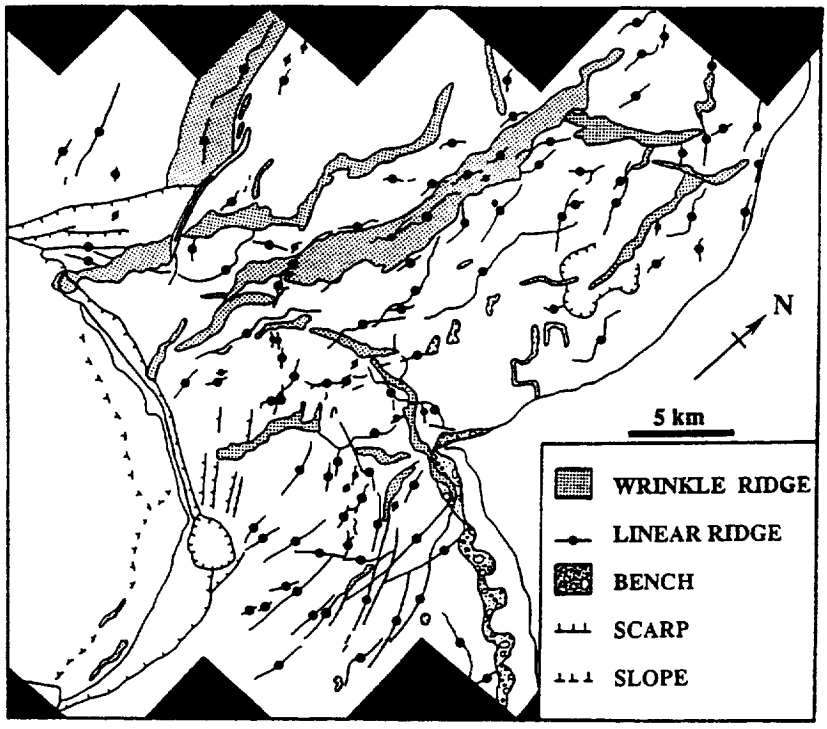

Fig. 3 (bottom): A complex series of linear ridges is seen on the floor of craters 4 and 5, indicating that a large over-turning lava lake may have existed soon after the initial collapse event. Note that these linear ridges are superposed upon the younger wrinkle ridges. See Fig. 1a for location. Mapped from Viking Orbiter frames 473S17 - 26.

Acknowledgement: The help of Eric Eliason at USGS Flagstaff in recovering the digital data used here for frame 860A68 is much appreciated.

Interpretation of Spectral Units of Isidis-Syrtis Major from ISM-Phobos-2 Observations. John F. Mustard[1], J-P. Bibring[2], S. Erard[2], E. M. Fischer[1], J. W. Head[1], S. Hurtrez[3], Y. Langevin[2], C. M. Pieters[1], C. J. Sotin[3] (1) Dept. Geol. Sci, Box 1846, Brown Univeristy, Providence RI (2) Institut d'Astrophysique Spatiale, 91405, Orsay France (3) Labratoire de Geodynamique Interne, 91405 Orsay, France

Introduction: During the encounter of Phobos-2 at Mars between January and March of 1989, imaging spectrometer data were obtained by the ISM instrument for several areas on Mars. These are the first high spectral and spatial resolution data for Mars and provide important information for identifying the composition of the atmosphere and surface (1). Data obtained for the Isidis-Syrtis Major region are examined here to determine and interpret the spectral features which characterize surface units defined in a companion abstract by (2). The area of the Martian surface covered by these data is shown in outline on the Viking orbiter photomosaic in Figure 1. A diverse range of geologic and geomorphic terrains are contained in this window and it is anticipated that careful analysis of these data will provide information on the composition of the Syrtis Major volcanic materials, basin rim materials of Isidis, and the cratered terrains of Arabia and Amenthes.

Unit Definition: Surface spectral units shown in the schematic map in Figure 2 were defined by (2) on the basis of spectral variation using the first 51 even channels. In this approach, each pixel in the image data is modelled as a linear combination of 2 endmembers chosen from within the window. One endmember is selected from the bright materials in the Isidis basin and one from the dark materials on the eastern part of Syrtis Major indicated by E1 and E2 in Figure 1. Pixels most accurately modelled by these endmembers (low total variance, random error as a function of wavelength) comprise the Isidis and Syrtis East units. The other units have high variance and/or show non-random variations in error as a function of wavelength (residual spectra). Careful examination of the residual spectra and the magnitude of the variance led (2) to define the other 3 units shown in Figure 2.

The correlation of the spectral units with the broad scale surficial geologic and geomorphic features is discussed in in detail by (2). Briefly, the Isidis unit is associated with bright deposits in the Isidis basin, the Cratered unit is associated with the rim of the Isidis basin, and the Arabia unit in the extreme north-west corner of the window corresponds with the edge of the cratered highlands. Two distinct units are recognized on the Syrtis Major plateau; an eastern and a western unit. Although the residual spectra are used to define these units, all spectral features identified are relative to the endmember spectra and direct compositional interpretations are difficult.

Calibration of ISM Spectra: The ISM data are initially calibrated using pre and inflight engineering data, an assumed average spectral response of Phobos and applying a preliminary atmospheric correction based on the strength of the 2.0 μm CO_2 absorption band (3). An additional calibration was applied to these data by assuming regions of homogeneous bright surface material have the same spectral properties as average bright terrain measured telescopically (4). Average telescopic data for bright regions were smoothed and resampled to ISM wavelengths. The region of the ISM data selected for this calibration is indicated by STD in Figure 1. This calibration approach is not an absolute measure of reflectance and subject to possible errors in the choice of reference spectra and the spectral properties of the surface calibrated to. This procedure surpresses features common to all surfaces but not in the reference spectrum.

Interpretation of Spectra Units: Typical spectra from each of the spectral surface units shown in Figure 2 are presented in Figure 3. The primary spectral features which distinguish these units are albedo, slope and the nature of the absorption band between 0.8 and 1.2 μm. The character of the absorption band is particularly important because it provides information regarding the composition of the surface. In the spectra of the bright terrain units, the band shape and position (near 0.9 μm) is relatively constant and is characteristic of Fe^{3+} absorptions observed in predominantly dust covered regions (4, 5). The primary spectral differences between the bright terrain units are the slope of the spectrum and slight variations in the position and shape of the 0.9 μm ferric absorption band. Whether the sources of the observed spectral variations are compositional, textural, or otherwise is unclear, however they do define spatially coherent units which are associated with morphologic and geologic features (2).

The shape and position of the absorption centered near 1.0 μm in the spectra of the Syrtis Major units is indicative of Fe^{2+} crystal field absorptions in mafic minerals. To de-emphasize albedo relationships and visually enhance absorption features, the spectral segments for the Syrtis Major units and the Isidis unit are divided by a simple straight line continua and are presented in Figure 4. The shape of the 1.0 μm band for the Syrtis units, and in particular the width of the bands, suggest that multiple mafic minerals contribute to the measured reflectance. In addition to the 1.0 μm band, there is a broad band centered near 2.1 μm. The presence of this feature together with the 1.0 μm band is strong evidence that high calcium pyroxene is present in the volcanic materials of Syrtis Major, the presence of which was previously proposed by (6) based on the shape of the 1.0 μm band alone. A principal distinguishing feature of the Syrtis Major units is the slope of the spectra towards long wavelengths; Syrtis East has

a decrease in reflectance towards longer wavelengths while Syrtis West is relatively flat. It is unknown at this time whether this is a weathering or surface coating phenomenon, or a fundamental mineralogic difference.

A significant degree of spectral variation exists in these data which was used to define units by (2). The principal distinguishing spectral characteristics between units are albedo, slope, and nature of the 1.0 μm band. In the units of Syrtis Major, the presence of clino pyroxene is clearly indicated as well as additional unresolved mafic mineral. We are currently in the processes of refining the calibration and also incorporating odd channels into the analysis to increase the spectral resolution and help resolve some of the remaining compositional ambiguities.

References: (1) Bibring et al, *Nature 341*, 1989. (2) Erard et al, *LPSC XXI* (this volume) 1990. (3) Erard et al, *Bull. Am. Astron. Soc. 21*, 1989 (4) McCord et al, *JGR 87*, 1982 (5) Singer, *JGR 87*, 1982 (6) Singer, *LPSC XI*, 1980.

Figure 1. Area covered by the ISM data for the Isidis-Syrtis Major window. The actual image is 26 by 116 pixels and a typical pixel to scale is indicated by the white arrow. The location for the reference spectra (E1 and E2) and the standard area (STD) are also indicated.

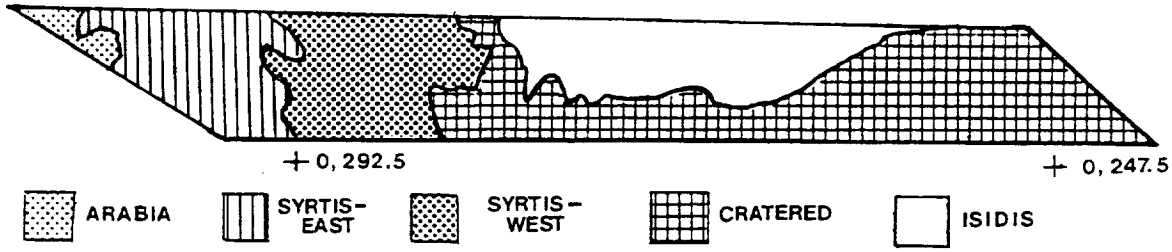

Figure 2. Schematic map for the above window of spectral units defined by (2) using the spectral characteristics of the first 51 channels of the ISM data.

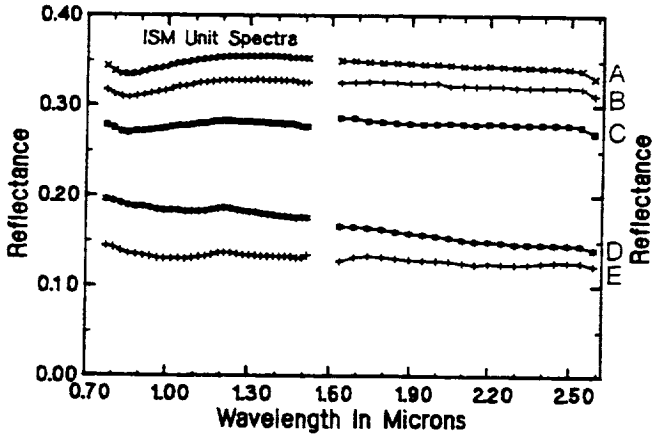

Figure 3. Calibrated ISM spectra typical of the units shown in Figure 2. A) Isidis B) Cratered Highlands C) Arabia D) Syrtis East E) Syrtis West.

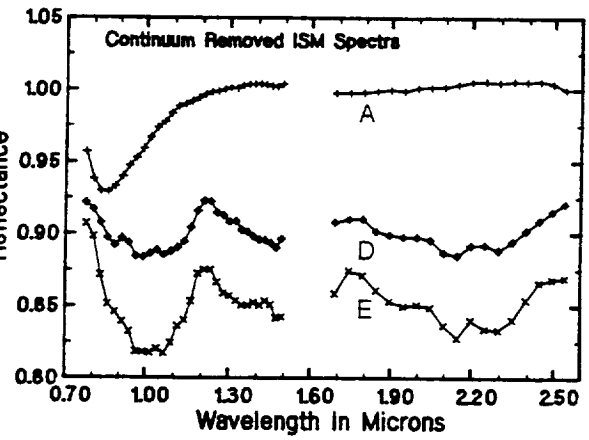

Figure 4. Spectra of the units Isidis (A), Syrtis East (B) and Syrtis West (C) after removing a simple straight line continuum for each segment. These spectra are offset 5% relative to each other for clarity.

IMPACT CRATERING ON MARS AND THE FORMATION OF CRATER LAKES: A POSSIBLE ENVIRONMENT FOR THE ORIGIN OF LIFE;

H.E. Newsom and G.E. Brittelle, Institute of Meteoritics and Department of Geology, University of New Mexico, Albuquerque, NM 87131.

Liquid water, required for the origin and growth of life, could have been present in two environments on Mars, lakes or in shallow groundwater, including near surface expressions of groundwater, such as springs. Under present climatic conditions on Mars, liquid water is not likely to exist in either environment. Liquid water on Mars requires either a warmer climate, which could have been present early in the history of Mars, or a source of heat, such as volcanism or impacts, which could be present throughout martian history. In this abstract we will discuss the effects of impacts and volcanism on the existence of liquid water on Mars, including the formation of crater lakes and liquid ground water systems. We will show that suitable environments for the origin of life on Mars may have existed, even in the absence of a significantly warmer climate in the past.

The large extent of biologic activity in groundwater systems on the Earth is well known [1]. The interaction of water or ice and hot rock due to volcanic activity could produce liquid groundwater even under present conditions on Mars. A similar environment near or within slowly cooling impact melt sheets, would have been common early in the history of Mars. Over the last ten years, an ongoing investigation of the hydrothermal alteration of impact melt sheets on the Earth has demonstrated that the presence of water plays an important role in the cooling of deposits containing impact melt [2]. Investigations of the cooling and alteration of suevite (melt-bearing breccia), at the Ries Crater in West Germany, has shown that most of the alteration and clay formation occurred during a long period of slow cooling below the boiling point of water [3]. Paleomagnetic techniques have confirmed that alteration and clay formation were probably connected with cooling of the melt sheet rather than being due to alteration under ambient conditions over the 15 m.y. since the formation of the crater [4]. On Mars, impact melt deposits outside of craters and basins could produce widespread shallow aquifers by melting of ground ice. Such shallow aquifers could even be connected with the formation of small valley networks on Mars [5]. The resulting small valleys may not even be closely associated with nearby craters because the distribution of impact melt from very large craters and basins may be very widespread and variable. Also, the liquid groundwater produced by melting ground-ice could flow for significant distances without a surface expression.

An even more important environment for biologic activity on Mars may be lakes, including impact craters which have become flooded with groundwater. The early presence of lakes in low lying areas such as Valles Marineris has been suggested as a site for biological activity [6]. An important question is whether such lakes would be liquid. McKay et al. [7] investigated the thickness of ice on perennially frozen lakes in the Antarctic and on Mars and the calculations for Mars were extended by Squyres [8]. Assuming present conditions, predicted ice thicknesses (> 200 m) are unlikely to allow liquid water to exist in martian lakes [8]. We have investigated the effects of heat from a cooling melt sheet, buried beneath a crater lake, on the thickness of ice on the surface of such a lake. As an example, we have used the calculated conductive cooling profiles for the 200 m thick impact melt sheet from the 65 km diameter Manicouagan crater in Quebec [9]. The calculated heat flow is shown in Fig. 1. This is compared with the other major source of heat within frozen lakes, the latent heat of freezing of water. The assumption is that the ice maintains an equilibrium thickness, with ablation from the surface and freezing at the ice-water interface [7]. Because of the low ablation rates expected for Mars under current conditions, this latent heat of freezing is much less than the heat from the melt sheet for the time interval indicated in the figures. The predicted thickness of ice on the crater lake, indicated in Fig. 2, will be less than 50 m for several thousand years, for ablation rates estimated by Squyres [8] for the present atmospheric pressure of 7 mbar. Eventually, as the heat from the melt sheet is lost, the thickness of the ice will increase to equilibrium values ranging from 200 m to 600 m for ablation rates of 3 cm/yr and 1 cm/yr respectively. Ablation rates higher than 3 cm/yr are unlikely under present conditions [8]. With atmospheric pressures as great as 300 mbar the ice thicknesses will be significantly less. The main conclusion from these calculations is that heat from a buried melt sheet will sustain a liquid crater lake for thousands of years, even under present climatic conditions on Mars. The duration of the cooling will undoubtedly be significantly shortened because of hydrothermal circulation of water through the melt sheet, but the existence of such crater lakes may still be recorded in the deposits within the craters.

Conclusions

Liquid groundwater or lakes could exist early in Martian history, even without a significantly warmer climate, with heat available from volcanism or impacts, especially from cooling melt sheets in large craters. Even though the liquid state of a martian crater lake would be short on an evolutionary time scale, hundreds of such lakes may have formed, including lakes within basins much larger than those modelled here. In addition, according to Stanley Miller [10], the time scales needed for the origin of life may be as little as 10^4 years. The dispersal of life-forms around Mars is also possible by impact processes, including spallation [11]. Other aspects of impacts that could be favorable to the origin of life include the possible presence of hot springs at the surface, within or near large craters associated with cooling melt sheets [5], the presence of shocked minerals, which could provide a source of chemical energy [12], and the formation of abundant clays and zeolites, which could catalyze organic reactions.

References

[1] Back Groundwater 27, 618-622, 1989. [2] Newsom Icarus 44, 207-216, 1980. [3] Newsom, Graup, Sewards, and Keil Proc. Lunar Planet. Sci. Conf. 17th, J. Geophys. Res. 91, E239-E251, 1986. [4] Iseri, Geissman, Newsom and Graup Abstracts for the 52nd Meteoritical Society Meeting, Lunar and Planetary Inst., p. 95, 1989. [5] Brakenridge, Newsom and Baker, Geology 13, 859-862, 1985. [6] McKay and Stoker Rev. Geophys. 27, 189-214, 1989. [7] McKay, Clow, Wharton, Jr., and Squyres Nature 313, 561-562, 1985. [8] Squyres Icarus, 1989. [9] Onorato, Uhlmann and Simonds, J. Geophys. Res. 83, 2789-2798, 1978. [10] Miller in Aspects of Chemical Evolution, John Wiley, 85, 1984. [11] Melosh Lunar and Planet. Sci. XVI, 550-551, 1985. [12] Boslough and Cygan Proc. Lunar Planet. Sci. Conf. 18, 443-454, 1988.

Figure captions

Fig. 1 The heat flow from a 200 m thick impact melt sheet has been estimated from the calculations of Onorato et al. [9] assuming a constant heat capacity. Even slower cooling times were obtained using a temperature dependent heat capacity [9].

Fig. 2 The ice thickness for two different assumptions about the ablation rate at the surface of the ice, which is assumed to be equal to the amount of ice crystallizing at the base of the ice. The solidification of the ice releases latent heat. The other parameters used in the calculation are: average temperature -43 °C, albedo 0.75, solar flux 180 W m^{-2}, extinction path length 1.0 m.

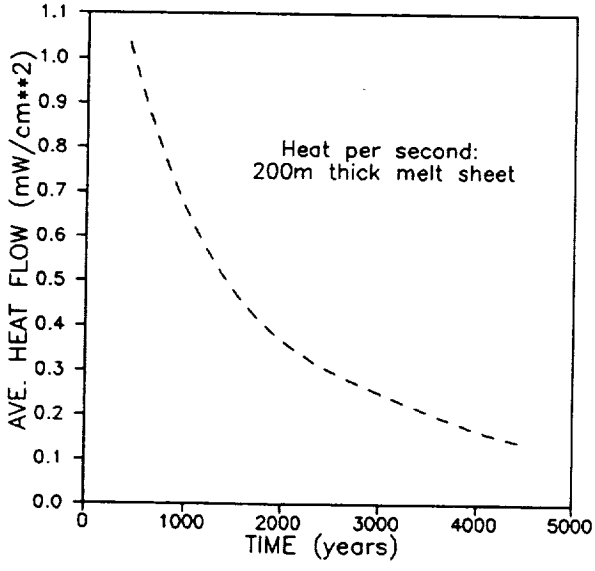

Figure 1

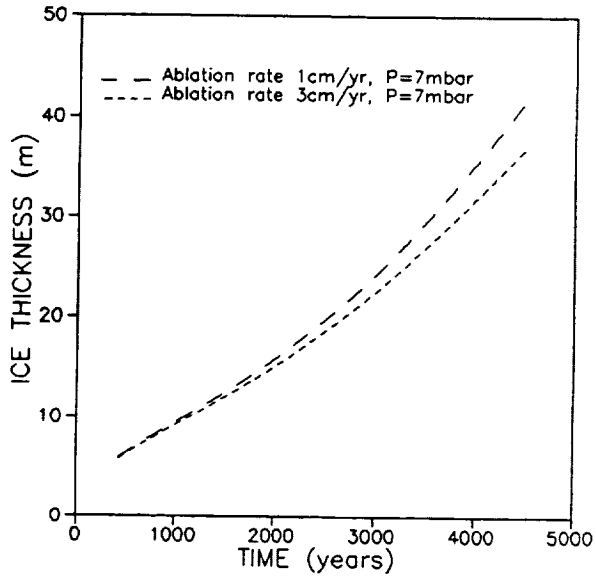

Figure 2

A MODEL FOR CHEMICAL EVOLUTION OF LIFE ON MARS, V. R. Oberbeck, NASA Ames Research Center, Moffett Field CA 94035, J. R. Marshall, Arizona State University, Tempe AZ 85287, D. E. Schwartz, SETI Institute, Mountain View, CA 94043

Geological and atmospheric models of Mars strongly suggest the presence of liquid water and a significant atmosphere prior to 3.8 Gyr. Early conditions favorable for life on Mars may have been similar to those on Earth at the time when life began on this planet. It has recently been recognized that the path of prebiotic chemistry (and of life itself) on the early Earth was probably interrupted, or at best retarded, by giant impacts[1]. The time between such impacts (just before the oldest evidence of life on Earth, 3.8 Gyr ago) has been used to estimate the maximum time required to originate life[2,3]. When the same calculations are applied to Mars, it appears that the time windows available for the development of life are longer than those for Earth[3]. Consequently, conditions on Mars conceivably could have been more favorable to life than were those on early Earth. Thus, Mars remains the most likely extraterrestrial setting for the origin of life. However, no specific model for *prebiotic* chemical evolution has yet been developed for Mars.

We now consider the geologic environment during Noachian time in order to develop a realistic model for the planetary processes that could have been involved in the chemical evolution of life on Mars. During the first 800 My of the Solar System, the terrestrial planets accreted planetesimals and experienced an exponential decay of impacting objects. Based on knowledge of the lunar uplands[4], impacting objects produced a thick megaregolith of crushed silicate minerals. Volatiles from comets were also delivered in sufficient quantities to produce terrestrial oceans similar in size to those present today and water, of exogenous origin, 10 m to 100 m in depth may have been retained on Mars[5] very early in its history. Because certain classes of meteorites contain clay minerals believed to have been formed in hydrated regoliths on planetary surfaces[6], we believe that it is likely that clay minerals existed in the ancient megaregoliths of both Mars and Earth. The existence of valley networks formed by sapping in the ancient cratered terrain suggests that surface water had a very limited distribution during the Noachian period. Intermittent precipitation fed subsurface aquifers which in turn fed springs at the heads of sapping channels formed by intermittent flowing water[7]. We believe that the geologic and meteorologic conditions during this period on Mars were at least as favorable (and perhaps more so) for the origination of life as they were on Earth.

We propose the following model for chemical evolution of life on Mars. Important prebiotic organic reactants were supplied by comets, IDPs, carbonaceous chondrites, and photochemical reactions.These compounds would have included amino acids, such as those recently discovered in clays at the KT boundary[8]. Monomers in the atmosphere were scavenged by precipitation or brought to the surface by sedimentation. During the time when reactants where incorporated in rain drops, some were polymerized to produce more complex prebiotic materials.

Seepage of these materials into the megaregolith then provided an ideal environment for the attachment of such monomers and polymers to clay particles. Percolation/filtration processes and fluctuating groundwater levels permitted dehydration of monomers and redistribution of reaction-product polymers. Fluctuations in water content are known to promote the formation of macromolecules[9]. Over a long period of time, the megaregolith acted as a large chemical processing column to form organic polymers of increasing complexity.

The next stage of biochemical organization, the formation of cell-like structures, occurred in the bottoms of sapping channels and lakes fed by sapping channels. Groundwater percolating through the megaregolith emerged as springs at the amphitheater heads of the channels. These were abundant on the surface of the ancient cratered terrain. Complex polymers emerging with the groundwater developed cellular organization on the level of coacervate droplets in this environment, and this permitted some interchange of biochemical compounds with the environment. Solar energy was available as an energy source to drive further chemical organization. Eventually, life may have originated in concentrated aqueous solutions at the bottoms of sapping channels and lakes in a way similar to that proposed for the terrestrial oceans.

Such a model for the chemical evolution of life on Mars compares favorably with the existing model for the origin of life on Earth. For this planet, life is believed to have originated in the primordial soup of organic compounds in the ocean. Monomers were produced in, or supplied to, the atmosphere in the manner referred to above and ultimately settled into the ocean. On Earth, the concentration of monomers in the oceanic "soup" would have taken longer than the time required to concentrate monomers in the megaregolith of Mars. In addition, movement of groundwater through the megaregolith would have provided more efficient absorption of monomers on clay particles. Thus, chemical evolution of life may have proceeded more rapidly on Mars.

References: (1) Maher K. A. and D. J. Stevenson (1988) *Nature* **331**, 612-614 (2) Oberbeck V. R. and G. Fogleman (1989a) *Origins of Life and Evolution of the Biosphere,* in press. (3) Oberbeck V. R. and G. Fogleman, (1989) *LPSC* **XX,** 800 (4)Aggarwal H. R. and V. R. Oberbeck (1978) *LPSC* **IX**, 829 (5) Chyba C. F. (1989) *Nature,* in press, Cornell University CRSR 930 revised. (6) Bunch T. E. and S. Chang (1980) *Geochim. Cosmochim. Acta* **44**, 1543 (7) Carr M. (1989) *Icarus* **79**, 311 (8) Cronin J. R. (1989) *Nature* **339**, 423 (9) Lahav N., D. White and S. Chang (1978) *Science* **201**, 67.

SEARCH FOR LIFE: A SCIENCE RATIONALE FOR A PERMANENT BASE ON MARS, V. R. Oberbeck, NASA Ames Research Center, Moffett Field CA 94035, J. R. Marshall, Arizona State University, Tempe AZ 85287, D. E. Schwartz and R. L. Mancinelli, SETI Institute, Mountain View CA 94043

Results of the Viking mission to Mars provided no compelling evidence for extant life, but oxidants could have masked evidence for biological activity[1]. The search for evidence that life originated on Mars remains a primary reason for further scientific exploration of the planet. Even if there was no extant life at the Viking sites, extant life may exist because most of the promising potential Martian habitats were not explored. It is noteworthy that prebiotic reactants and liquid water probably existed at the surface until about 3.8 Gyr ago(2). During this period, Mars was subject to impacts that would have frustrated the origin of life. The time available between these planet-sterilizing events was longer than the time required to originate life on Earth[2]. Thus, there would have been sufficient time for life to originate on Mars before 3.8 Gyr ago. If life existed, it may either have become extinct at the surface, leaving behind fossils, or migrated into the groundwater after 3.8 Gyr ago. This implies that evidence for extant life should be sought beneath the surface and that evidence of extinct life should be sought in the older surface terrain. Mars remains the most promising extraterrestrial setting where life may have originated. The discovery of evidence for either extant or extinct life on Mars would profoundly affect mankind because it would suggest the possibility that life may have originated in many other places in the universe.

The National Research Council recommended searching for four types of indirect evidence for extant life during space missions. These include liquid water, organic compounds, electrolytes, and biogenic gases. However, they point out that none of these is proof that life exists. Conclusive evidence for life cannot be sought with Viking style missions(3) that search for these types of evidence nor do we believe can it be sought with other types of unmanned craft. For example, penetrators could conceivably deploy instruments that could search for this indirect evidence of extant life beneath the surface, but penetrators can only deploy limited payloads to a limited depth in a limited number of places. At best, the results obtained would only provide inconclusive evidence for life on Mars. Therefore, we believe that the search for extant life beneath the surface will be difficult indeed. The search for fossil evidence of life at the surface will also be extremely difficult to undertake. Such fossil evidence is likely to be very old[2] and the volume ratio of fossils to rock will probably be very small; only a centimeter layer of fossiliferous material may exist in hundreds of meters of sedimentary rock. The search for such layers could be quite time-consuming and would require the knowledge and experience of a well-trained geologist. Artificial intelligence techniques that could be used on unmanned surface vehicles (e.g., rovers) could easily mistake inorganic artifacts for fossil remains.

Because the positive results of a search for conclusive evidence for life on Mars would have profound implications for mankind, and because of the difficulties inherent in the search, we believe that this search is compelling justification for a permanent science base on Mars. In the event that extant organisms are found, a semi-permanent presence permits examination of extant life forms in order to prevent possible harmful forward and backward contamination. It is recognized that the same results may be achieved in carefully prepared clean rooms and planetary protection facilities on Earth, a semi-permanent facility on Mars would provide added protection of great value. Additionally, if extant lifeforms are found, they are best studied *in situ*.

The search for extant life should concentrate on subsurface locations. The disappearance of an appreciable atmosphere and associated liquid surface water about 3.8 Gyr ago[4,5] may imply that organisms, as we know them, could not now exist at the surface. It has recently been discovered that a large biomass of microorganisms extends to great depths within terrestrial aquifers[6] and Mars may have analogous environments. However, great effort must be expended in searching for such organisms and in keeping the samples pristine. On Mars, it may be

possible to sample groundwater at selected sites near sapping channels. This would require complex drilling operations in rugged Martian terrain that can only be performed by humans in semi-permanent bases with laboratory facilities. Also, the careful field analysis of groundwater systems, required before extensive drilling is done, is not possible with unmanned landers.

The search for fossil evidence of past Martian life will require painstaking field analysis and detailed examination. Long drill cores may need to be examined, and large volumes of debris searched, for minute traces of extinct life. It is difficult to envision how a successful search for fossils could be carried out without preliminary geological field surveys followed by exhaustive on-site laboratory investigations.

A careful examination of ecosystem dynamics can only be accomplished by humans inhabiting a Mars base equipped with a laboratory. Interrelationships between organisms and their environments are so complex that one is compelled to study organisms in their natural habitat. For example, two elements that are important to organisms are nitrogen and sulfur. In terrestrial ecosystems, we know that cycling of these elements requires a community of co-existing organisms working in concert with the environment. Changing the environment leads to significant changes in the cycling. The types of *in situ* studies that would be required to determine biogeochemical cycles in these ecosystems would be virtually impossible with robotic missions. Such studies, performed by scientists on the surface of Mars, will expand our knowledge of nutrient cycling in an extraterrestrial planetary context. If we can learn how an extraterrestrial biota interacts with its environment, it would greatly expand our knowledge of the limits that planetary environments place on the existence of life. This, in turn, would provide additional evidence regarding the possibility of life elsewhere in the universe. The history of comparative planetology tells us that it is precisely the opportunity for the study of physical and chemical processes in different planetary settings that has offered completely new insights into planetary processes acting within our own terrestrial environment. The presence of humans in a semi-permanent base on Mars will permit similar new perspectives on the importance of processes that are integral with the possibly of origination of life elsewhere.

References: (1) Klein H. P. (1978) *Icarus* **34**, 666 (2) Oberbeck V. R. and G. Fogleman (1989) *LPSC* **XX**, 800 (3) Hartman H., J. G. Lawless and P. Morrison (eds.) (1985), NASA SP-477. (4)Carr M. H. and G. D. Clow (1981) *Icarus* **48**, 91-117 (5) Pollack J. B., J. F. Kasting and S. M. Richardson (1987) *Icarus* **71**, 203-224 (6) Phelps T. J., E. G. Raione, and D. C. White (1988) U. S. Dept. of Energy, DP-MS-88-100.

STABILITY, COMPOSITION AND PHASE RELATIONS OF MARTIAN MANTLE CARBONATES

Maria Odezynskyj, Dept. Geo., ASU, Tempe, AZ 85287-1404, John R. Holloway, Depts. Chem. and Geo., ASU, Tempe, AZ 85287-1404.

This abstract introduces further results from a study of Martian mantle carbonates: their stability and composition, and qualitative information about their phase relations during a partial melting event. Data were collected from piston-cylinder experiments conducted on model Martian mantle compositions at 25 kb. and a range of temperatures from 1150°C to 1250°C. Graphite lined Pt capsules were loaded with a basalt + dolomite mixture which was sandwiched between peridotite + basalt + dolomite. The peridotite was composed of synthetic olivine, ortho- and clinopyroxenes, all with mg# 75 (atomic Mg/(atomic Mg + atomic Fe)); natural garnet with mg# 74; natural basalt with mg# 50; and a pure, natural dolomite. Run times were 24 hours. Oxygen fugacity conditions, calculated from Fe solution into Pt (Gudmundsson and Holloway, 1989), are constrained to be within ± 0.9 $\log_{10}$ units relative to NiNiO at 1 atm. and run temperature.

The carbonates in this study fall into two compositional categories. The first, a water soluble 'alkali' carbonate, is present in all experiments at temperatures < 1250°C; its approximate composition is given in Table 1. Figure A is a backscatter image of a region containing the carbonate. Its texture and occurrence suggest that it could be a quench product of an alkali carbonate liquid. Such an interpretation is consistent with the results of Wallace and Green (1988). In contrast, a Ca-Mg-Fe carbonate crystal phase has a stable appearance (see Figure B) up to a temperature between 1200°C and 1225°C. X-ray diffraction studies and Transmission Electron Microscopy indicate that this carbonate has a calcite structure. Above the given temperature range, Mg-Fe calcite contains veins of alkali carbonate and frequently occurs near vugs. (See Figure C.) The average composition of the calcite at different temperatures is given in Table 2.

Silicate phases present in the run products are: olivine, pyroxenes, garnet $\pm$K feldspar. Also present is fine-grained silicate material with a texture and composition that suggest a melt phase. Distinct regions of quench crystals may represent immiscibility between the silicate and carbonate liquids up to ≈1250°C. Average structural formulae of the minerals are listed in Table 3. The Fe/Mg partitioning among phases varies: e.g. 2.27 between cpx and gt, or 0.08 between opx and cpx, in a 25 kb, 1200°C run. (Values from 21st run.) An approach, rather than achievement, of equilibrium is apparent from a comparison of the experimental partitioning with published values. Ellis and Green, 1979, report 2.26 for Fe/Mg partitioning between cpx and gt, and Mori and Green, 1978, report 0.93 for opx and cpx under comparable P and T conditions.

At temperatures $\leq$ 1200°C, alkali carbonate 'melt' coexists with Mg-Fe calcite. Microprobe analyses (see Table 2) show that alkalis do not readily enter the calcite structure. Falloon and Green (1989) approximated the solidus for alkali carbonate at ≈1025°C at 25 kb. Our data place the Mg-Fe calcite solidus between 1200-1225°C at 25 kb. These observations suggest a eutectic melting relationship for mantle carbonates as shown in Figure D.

References:

Ellis D J and Green D H (1979) Contrib Min Pet **71** 13. Falloon T J and Green D H (1989) EPSL **94** 364. Gudmundsson G and Holloway J R (1989) EOS **70** 1402. Mori T and Green D H (1978) Jour Geo **86** 83. Wallace M E and Green D H (1988) Nature **335** 343.

MARTIAN MANTLE CARBONATES

Odezynskyj, M. and Holloway, J. R.

Table 1
Alkali Carbonate 'Melt' Composition

	1200°C	1225°C
SiO2	5.5	6.5
TiO2	1.2	1.9
Al2O3	0.5	0.6
FeO	23.4	18.7
MnO	0.1	0.1
MgO	11.2	10.3
CaO	8.0	10.2
Na2O	3.7	5.6
K2O	7.1	5.1
P2O5	9.4	9.9
(diff) CO2	30.0	31.4
mg#	32.4	35.5

Table 1: Averaged compositions (in weight percent) of alkali carbonate. 1200°C values from 21st run; 1225°C values from 19th run.

Table 2
Average Compositions of Mg-Fe Calcite

	1175°C	1200°C	1225°C	1250°C
SiO2	0.02	0.36	0.04	0.21
TiO2	0.01	0.13	0.04	0.04
Al2O3	0.02	0.04	0.03	0.06
FeO	5.81	10.49	10.96	11.18
MnO	0.01	0.13	0.12	0.14
MgO	10.33	12.37	12.40	13.05
CaO	41.95	33.58	32.32	33.29
Na2O	0.02	0.20	0.16	0.18
K2O	0	0.44	0.18	0.26
P2O5	n/a*	0.73	0.44	0.41
(diff) CO2	41.85	41.53	43.30	41.18

Table 2: Averaged compositions (in weight percent) of Mg-Fe calcite. 1175°C values from 5th run; 1200°C from 21st, 1225°C from 19th and 1250°C from 20th runs.

* -not analyzed

Table 3
Structural Formulae of Run Product Silicates

phase	structural formula
	1175°C (run 5)
olivine	$Mg_{1.47}Fe_{0.55}Si_{0.98}O_4$
l.c.pyx*	$Na_{0.01}Al_{0.06}Ca_{0.02}Mg_{1.47}Fe_{0.46}Si_{1.93}O_6$
clinopyx	$Na_{0.0}Al_{0.0}Ca_{1.01}Mg_{0.92}Fe_{0.14}Si_{1.96}O_6$
garnet	$Ca_{0.69}Mg_{0.82}Fe_{1.57}Al_{2.06}Si_{2.89}O_{12}$
	1200°C (run 16)
olivine	$Mg_{1.52}Fe_{0.53}Si_{0.97}O_4$
l.c.pyx*	$Na_{0.01}Al_{0.02}Ca_{0.08}Mg_{1.58}Fe_{0.38}Si_{1.95}O_6$
clinopyx	$Na_{0.03}Al_{0.03}Ca_{0.68}Mg_{1.05}Fe_{0.29}Si_{1.96}O_6$
garnet	$Ca_{0.92}Mg_{0.69}Fe_{1.38}Al_{1.88}Si_{2.75}O_{12}$
	1225°C (run 13)
olivine	$Mg_{1.46}Fe_{0.53}Si_{1.00}O_4$
l.c.pyx*	$Na_{0.01}Al_{0.01}Ca_{0.14}Mg_{1.44}Fe_{0.43}Si_{1.98}O_6$
clinopyx	$Na_{0.02}Al_{0.03}Ca_{0.55}Mg_{1.11}Fe_{0.32}Si_{1.98}O_6$
garnet	$Ca_{0.84}Mg_{0.75}Fe_{1.36}Al_{1.91}Si_{2.95}O_{12}$

*l.c.pyx = low calcium pyroxene

Figure A: Alkali Carbonate 'Melt'

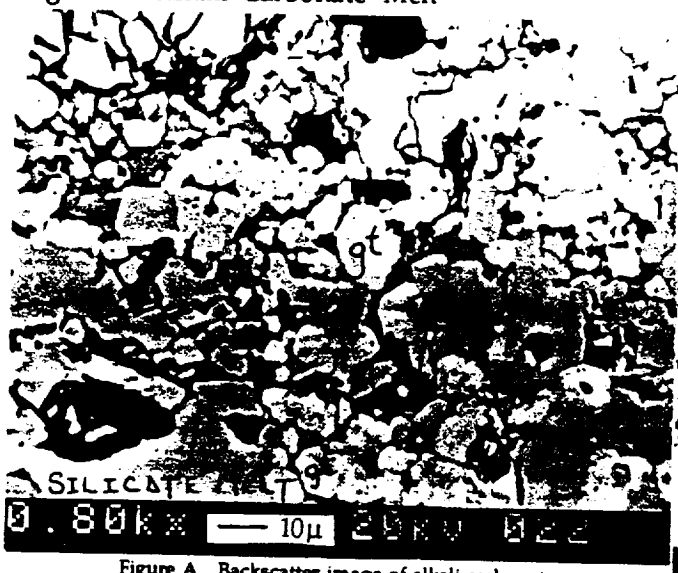

Figure A. Backscatter image of alkali carbonate melt. See text for discussion.

Figure C: Quenched Mg-Fe Calcite

Figure C. Quenched Mg-Fe calcite with veins of alkali carbonate.

Figure B: Stable Mg-Fe Calcite

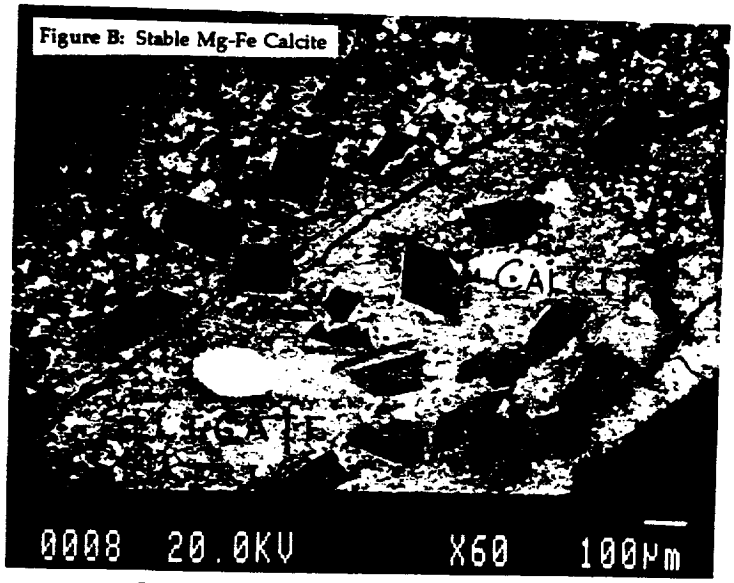

Figure B. Backscatter image of Mg-Fe calcite crystals within run product.

Figure D

A Schematic Diagram of Mantle Carbonate Phase Relations at 25 kb.

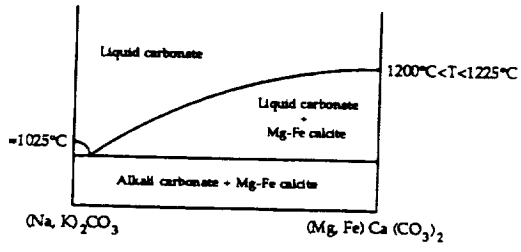

Figure D: Schematic projection of carbonate melting relations onto the alkali carbonate–Mg-Fe calcite join. Silicate relations not shown, but this diagram is for a phase assemblage which includes olivine, two pyroxenes and garnet.

SPECTRAL EMISSIVITY OF THE SILVER AND LUNAR LAKE PLAYAS - RELEVANCE TO ANALYSES OF MARS TIR DATA; S.B.Petroy and R.E.Arvidson, McDonnell Center for the Space Sciences, Earth and Planetary Sciences Department, Washington University, St.Louis, MO, 63130

Analyses of existing Viking IRTM data have focussed on providing broad compositional and textural constraints for martian sediments. The higher spectral and spatial resolution data to be acquired from the upcoming MO-TES mission will help to narrow these constraints, thus allowing for more detailed mapping of the martian surface. To prepare for these data, portions of two remote sensing field experiments (MFE-1988, GRSFE-1989) [1,2] were conducted to test procedures used to extract surface property information from TIR data. What follows is a report of initial results from the analyses of Thermal Infrared Multispectral Scanner (TIMS) data, field emission spectra, and field observations with respect to the physical characteristics (composition, emissivity, etc.) of two playas in CA and NV. These areas were selected because they are small and fairly homogeneous, but exhibit variability in surface texture and composition.

Silver Lake, north of Baker, CA, is bounded on the west by the Soda Mtns. The western shore of the playa consists of beach ridges and wave cut cliffs; the eastern shore is marked by a well-sorted quartz sand berm. The 26 km^2 floor of Silver Lake is fairly flat but slopes gently to the south. Lunar Lake, 100 km east of Tonopah, NV, is bounded to the northeast by the Lunar Crater Quaternary basaltic flows and tephra cones and to the southwest by uplifted Tertiary ryholite tuffs. The western shore of the playa abuts volcanic flows and tephra cones while the remaining shoreline is marked by a well sorted, quartz-rich sand berm. The floor of the playa is ~10 km^2 and is also extremely flat. Several areas at the southern end of the playa are covered with locally derived basaltic cobbles (2-10 cm). Both playas consist of fine-grained, hardpacked silt and clay, but vary widely in degree of compaction and mud-crack morphology.

In February and July of 1989, emission data were collected at both playas with the JPL Portable Field Emission Spectrometer (PFES) [3]. In addition, data were collected at the Cima basalt flows (CA) and Kelso dunes (CA) to provide information on compositional endmembers (see Figure 1).

The emissivity of the Kelso sample is typical for quartz-rich sands with an absorption minima centered near 9.0 μm [4]. Generally, the depth and position of the absorption minima shifts from left to right as the total silicate content within the sample decreases. This trend is observed in the Cima spectra; the emission curve of the I-flow (youngest) is typical of basalts with an absorption minima centered near 10.0 μm. The remaining flow surfaces are older and have accretionary mantles of aeolian sediments. This added silicic material pulls the overall emission curve down and shifts the minima more to the left.

Emission spectra were collected at two sites on Silver Lake - site 1 (south) consists of fine-grained clays (20-40 μm) and deep mudcracks and site 2 (north) of slightly coarser sediments and shallow mudcracks. The emission curves for Silver Lake are higher and flatter than the Kelso curve, and exhibit broad absorptions around 9.0 μm characteristic of fine-grained, quartz-rich materials [4]. The emissivity of site 2 exhibits a deeper absorption at 9.0 μm which is probably due to the slightly coarser nature of the sediment. At Lunar Lake emission spectra were collected at three sites - sites 1 and 3 consist of fine-grained clays and shallow mudcracks and site 2 of basaltic cobbles overlying the playa surface. The cobble site emissivity is similar to that of the Cima mantled flows; the absorption minima is broad and centered between 9.0 and 10.0 μm. The two playa sites exhibit essentially identical emissivities but show a marked contrast from the Silver Lake emission curves. The sediments at Lunar Lake appear to contain a significant mafic component which results in a broader emissivity minima and higher values at smaller wavelengths.

These field observations can be empirically related to color composites using TIMS bands 1, 3, and 5. The green areas on both images correspond to the wettest and lowest

points on the playas; they consist of the finest clays, deepest mudcracks, and densest vegetation cover. At Silver Lake, the general color trend across the lake (west-east) is light blue and red grading into purple, suggesting an overall decrease in particle size away from the source (Soda Mtns). The reddish tint across the lake is due to the more silicic origin of the clays. In constrast, Lunar Lake is dominantly purplish-red due to the more mafic origin of the clays. The red rims around both playas correspond to the well-sorted, quartz rich sands berms observed in the field.

Based on qualitative interpretations of the TIMS data and the field emission spectra, subtle compositional and textural differences across the two playas can be recognized. The next phase of this study is to model the data to more precisely estimate the texture and composition of these surfaces.

References

[1] Wall, S., et al. (1988) Bull. Am. Astr. Soc., 20, p. 809. [2] Arvidson, R.E. and D.L. Evans (1989) GSA Abst. with Prog., p. A121. [3] Hoover, G. and A.B. Kahle (1987) Phot. Eng. and Remote Sen., vol.53, p. 627-632. [4] Conel, J.E. (1969) JGR, vol.74, p.1614-1634.

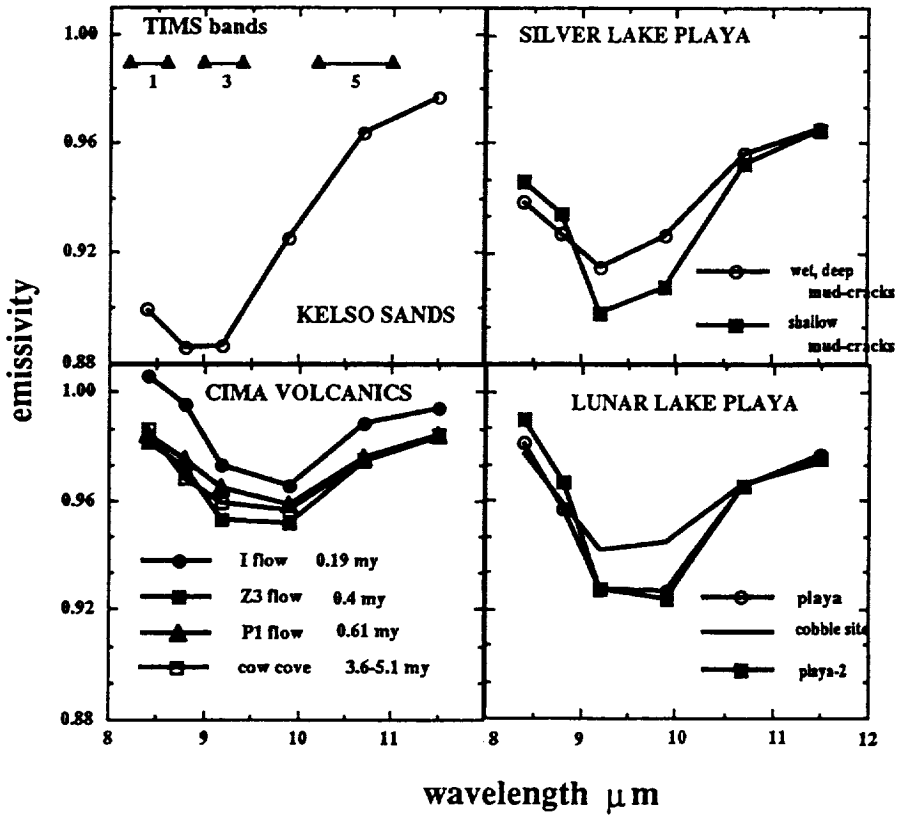

Figure 1. PFES data resampled into TIMS bandpasses and plotted as emissivity against wavelength.

EROSIONAL LANDFORMS AND MORPHOTECTONIC DEVELOPMENT IN VALLES MARINERIS (MARS): MELAS CHASMA; J.P. Peulvast, Laboratoire de Géographie Physique, CNRS, F 92195 Meudon, France.

Evaluating the respective influences of erosional and tectonic processes in the formation of the Valles Marineris troughs is decisive in their widened parts, where long wall segments display arcuate or irregular patterns which are not clearly related to faults (e.g. South Melas Chasma). Nevertheless strong tectonic control on the outlines of the walls and of the "bench" (layered rock plateaus) margins inside the troughs has been suggested in Candor and Melas Chasmata (1). By constructing detailed morphological maps (2), geological cross-sections and block-diagrams (fig. 1) it is possible to obtain more precise data on morphostructural and tectonic patterns in the same area.

The high dissected wall that overlooks the floor of Melas Chasma, i.e. the northern part of the trough, is controlled by faults west of Melas Labes, as demonstrated by stepped patterns with oblique hanging valleys or gullies. A downfaulted part of the main plateau forms a low bench above the floor (3). East of Melas Labes wide steps were probably faulted below a slightly arcuate wall but later landslides prevent easy identification of fault lines. WNW-ESE faults control the northern wall of Coprates Chasma (4), with hanging landslide scars developed from a probable former pit chain intersected after exaggeration of the fault scarp. Though wall rock remnants or small eroded horsts, occur in West Coprates Chasma, low mesas and alternate smooth and mottled surfaces in NW Melas Chasma seem to be underlain by layered deposits, surmounted by a few volcanic hills.

Thick layered deposits are more easily identified in the bench of South Melas Chasma, whose surface is 2-3 km or more above the floor. Whatever their origin is (volcanic, sedimentary or both: 5), the beds were formed in a confined area, during or after basin formation (which implies a subsidence of 6 or 7 km at least in SW Melas Chasma). Dissected walls and a few younger landslide scars overlook this 135 km wide bench or a deep discontinuous moat (SE Melas Chasma). Except in this last case the deposits extend into arcuate reentrants and embayments in the Sinai Planum edge, where no fault can be identified in spite of local parallelism with the Nia Fossae grabens. The SN ridge protruding from this edge is an erosional remnant of the plateau. It is therefore probable that wall backwearing occurred during the basin beds emplacement, even if complex downfaulting of blocks along oblique directions prepared this configuration (1).

The contrast between the southern and northern walls of Melas Chasma is best explained by later tectonic movements (downthrow: 1 or 2 km) along the continuations of the main faults of Ius and Coprates Chasmata through Melas Chasma, with a slight dextral offset. The faulted northern wall faces the bench margin,which appears as a fault scarp, especially if basin beds also underlay the floor: little or no erosion seems to be involved in the formation of this lower part (which would be the case if wall rock remnants were found in it, as suggested by (1).

Downfaulting of the floor, and possibly of parallel and oblique grabens inside the present bench and moat of SE Melas Chasma, resulted in landslides in the exaggerated northern wall (Melas Labes-Coprates Chasma) and in limited dissection and retreat of the edges of interior tectonic blocks, accompanied by differential erosion in alternate soft and hard layers. The occurrence of multiple cuesta-like bluffs and anticlinal hollows (east of the SN ridge) implies the presence of other structures: a long NW-SE monocline along the margin, possibly formed along the former edge of a southern deeper part of the basin before tectonic inversion, and several widely spaced NNW-SSE shallow synclines and low anticlines which formed only in the basin beds, probably as a response to differential vertical movements or strike-slip with weak compressional component in the narrow and weakened offset zone between Ius and Coprates Chasmata.

These deformations seem to predate the late faulting. They probably began during the formation of basin beds or its last stages, as suggested by possible unconformities and flexuring along wall contacts (SW Melas Chasma). They might be partly related to an old stage of volcano-tectonism (6) in a complex of caldera-like depressions along a wide graben or fracture set; deflection of Tharsis radial grabens around Melas Chasma (Nia Fossae) might be the same as observed around Alba Patera or Syria Planum. The basins were partly filled by volcanics and waste from highly erodable walls. Nevertheless this accumulation did not compensate subsidence and erosion induced by heating of volatile-rich wall rocks or tensional fracturing at depth (7).

Late faulting occurred mainly along the Ius-Coprates faults, i.e. in the northern half of Melas Chasma, resulting in increased total trough volume but also in narrowing of the main zone of tectonic activity, which became a simple graben with limited volcanism. Erosional widening became much less efficient than during the first stages, with a few landslides and limited erosion of faulted basin beds, probably for environmental as well as geological reasons (decreasing thermal activity and volatile content of wall rock, lithology of basin beds). Such a multistage tectonic activity probably occurred in the whole trough complex.

References: (1) Lucchitta 1989, LPSC XX, 590; (2) Peulvast and Costard 1989, LPSC XX, 840; (3) Witbeck et al 1988, USGS MIS Map I-XXXX, 55 p; (4) Schultz and Frey 1989, 4th Int. Conf. Mars, 183; (5) Nedell at al 1987, Icarus 70, 409; (6) Lucchitta 1987, LPSC XVIII, 572; (7) Tanaka and Golombek 1989 19 LPSC Proc. 383.

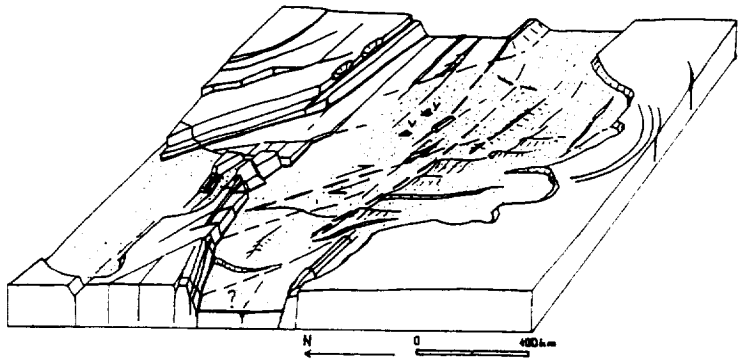

Figure I.The last morpho-tectonic stage in Melas Chasma. Dots: basin beds.